Electronic Supplementary Material (ESI) for Catalysis Science & Technology.
This journal is © The Royal Society of Chemistry 2023

Supporting Information

Catalysis of surface dispersed Cu^{2+} species on *t*-ZrO_2: Square-planar Cu catalyzed cross-coupling of arylboronic acid and imidazole

Masaru Kondo,*[1] Tatsuya Joutsuka,*[1,2] Kakeru Fujiwara,[3] Tetsuo Honma,[4] Masahiko Nishijima,[5] Shohei Tada*[6]

[1]*Department of Materials Science and Engineering, Graduate School of Science and Engineering, Ibaraki University, 4-12-1 Naka-narusawa, Hitachi-shi, Ibaraki 316-8511 Japan*

[2]*Frontier Research Center for Applied Atomic Sciences, Ibaraki University, Tokai, Ibaraki 319-1106, Japan*

[3]*Department of Chemistry and Chemical Engineering, Yamagata University, Yamagata 992-8510, Japan*

[4]*Japan Synchrotron Radiation Research Institute, Hyogo 679-5198, Japan*

[5]*Flexible 3D System Integration Lab, SANKEN, Osaka University, Mihogaoka, Ibaraki-shi, Osaka 567-0047, Japan*

[6]*Department of Applied Science and Engineering, School of Engineering, Hokkaido University, Kita 13, Nishi 8, Kita-ku, Sapporo, Hokkaido 060-8628, Japan*

Correspondence: masaru.kondo.fg74@vc.ibaraki.ac.jp
tatsuya.joutsuka.joe@vc.ibaraki.ac.jp
shohei.tada.st@eng.hokudai.ac.jp

CONTENTS:

Characterization of compounds …… SI-2

Characterization of catalysts…… SI-5

Computational details of DFT calculations …… SI-9

Control experiment …… SI-11

References …… SI-12

^{1}H-, ^{13}C NMR charts …… SI-13

Characterization of Compounds

^{1}H-, ^{13}C-NMR spectra were recorded with a Bruker AVANCE III (^{1}H-NMR 400 MHz, ^{13}C-NMR 100 MHz). ^{1}H-NMR spectra are reported as follows: chemical shift in ppm relative to the chemical shift of $CHCl_3$ at 7.26 ppm, integration, multiplicities (s = singlet, d = doublet, t = triple, m = multiplet), and coupling constants (Hz). ^{13}C-NMR spectra reported in ppm relative to the central line of triplet for $CDCl_3$ at 77 ppm. Column chromatography on SiO_2 was performed with Kanto Silica Gel 60 (40-100 μm). Commercially available organic and inorganic compounds were used without further purification.

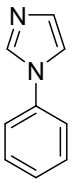

3a

3a: 21.8 mg, 76% yield; ^{1}H-NMR (400 MHz, $CDCl_3$) δ 7.85 (s, 1H), 7.48-7.45 (m, 2H), 7.38-7.35 (m, 3H), 7.27-7.26 (m, 1H), 7.19 (s, 1H); ^{13}C-NMR (100 MHz, $CDCl_3$) δ 137.2, 135.5, 130.1, 129.8, 127.5, 121.4, 118.2.

^{1}H and ^{13}C NMR charts were consistent with previously reported data.[1]

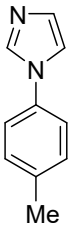

3b

3b: 29.3 mg, 93% yield; ^{1}H-NMR (400 MHz, $CDCl_3$) δ 7.82 (s, 1H), 7.25-7.22 (m, 5H), 7.19 (s, 1H), 2.38 (s, 3H); ^{13}C-NMR (100 MHz, $CDCl_3$) δ 137.4, 135.0, 130.3 121.4, 118.55, 20.9 (two peaks were overlapped).

^{1}H and ^{13}C NMR charts were consistent with previously reported data.[1]

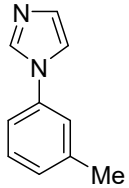

3c

3c: 31.2 mg, 99% yield; ^{1}H-NMR (400 MHz, $CDCl_3$) δ 7.83 (s, 1H), 7.34 (t, *J* = 7.6 Hz, 1H), 7.26 (d, *J* = 3.6 Hz, 1H), 7.18-7.15 (m, 4H), 2.41 (s, 3H); ^{13}C-NMR (100 MHz, $CDCl_3$) δ 140.0, 137.3, 135.5, 130.2, 129.6, 128.2, 122.1, 118.5, 118.2, 21.3

^{1}H and ^{13}C NMR charts were consistent with previously reported data.[2]

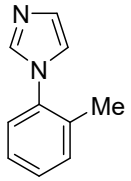

3d

3d: 24.0 mg, 76% yield; ^{1}H-NMR (400 MHz, $CDCl_3$) δ 7.58 (s, 1H), 7.36-7.20 (m, 5H), 7.06 (s, 1H), 2.19 (s, 3H); ^{13}C-NMR (100 MHz, $CDCl_3$) δ 137.4, 136.6, 133.8, 131.2, 129.3, 128.8, 126.8, 126.5, 120.4, 17.6

^{1}H and ^{13}C NMR charts were consistent with previously reported data.[1]

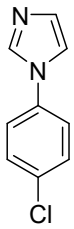

3e

3e: 25.2 mg, 71% yield; ^{1}H-NMR (400 MHz, $CDCl_3$) δ 7.81 (s, 1H), 7.45 (d, J = 8.8 Hz, 2H), 7.33 (d, J = 8.8 Hz, 2H), 7.22 (m, 2H); ^{13}C-NMR (100 MHz, $CDCl_3$) δ 135.9, 135.5, 130.7, 130.0, 122.7, 118.2

^{1}H and ^{13}C NMR charts were consistent with previously reported data.[1]

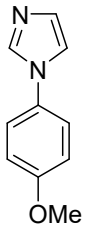

3f

3f: 26.8 mg, 77% yield; ^{1}H-NMR (400 MHz, $CDCl_3$) δ 7.75 (s, 1H), 7.30 (d, J = 8.8 Hz, 2H), 7.20-7.17 (m, 2H), 6.98 (d, J = 8.8 Hz, 2H), 3.85 (s, 3H); ^{13}C-NMR (100 MHz, $CDCl_3$) δ 158.9, 135.8, 130.7, 129.9, 123.2, 118.7, 114.9, 55.5

^{1}H and ^{13}C NMR charts were consistent with previously reported data.[1]

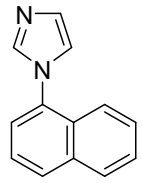

3g

3g: 29.8 mg, 77% yield; ^{1}H-NMR (400 MHz, $CDCl_3$) δ 7.95 (d, J = 7.8 Hz, 2H), 7.78 (s, 1H), 7.62-7.50 (m, 4H), 7.45 (dd, J = 7.2, 1.1 Hz, 1H), 7.38-7.22 (m, 2H); ^{13}C-NMR (100 MHz, $CDCl_3$) δ 134.1, 134.0, 129.6, 129.4, 129.2, 128.2, 127.5, 126.9, 125.1, 123.6, 122.2 (two peaks were overlapped).

^{1}H and ^{13}C NMR charts were consistent with previously reported data.[2]

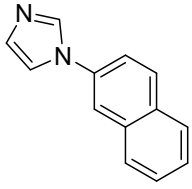

3h

3h: 31.5 mg, 81% yield; ^{1}H-NMR (400 MHz, $CDCl_3$) 7.97-7.94 (m, 2H), 7.89-7.86 (m, 2H), 7.80 (d, J = 2.2 Hz, 1H), 7.58-7.50 (m, 3H), 7.39 (s, 1H), 7.26 (s, 1H); ^{13}C-NMR (100 MHz, $CDCl_3$) δ 135.8, 134.7, 133.5, 132.1, 130.5, 130.0, 127.8, 127.7, 127.3, 126.5, 120.2, 119.0, 118.4

^{1}H and ^{13}C NMR charts were consistent with previously reported data.[2]

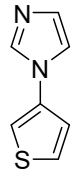

3i

3i: 11.1 mg, 37% yield; ^{1}H-NMR (400 MHz, $CDCl_3$) δ 7.81 (s, 1H), 7.43 (dd, *J* = 5.2, 3.2 Hz, 1H), 7.23 (s, 1H), 7.21-7.20 (m, 1H), 7.18-7.16 (m, 2H); ^{13}C-NMR (100 MHz, $CDCl_3$) δ 136.3, 135.8, 130.0, 127.1, 121.4, 118.5, 113.2.
^{1}H and ^{13}C NMR charts were consistent with previously reported data.[3]

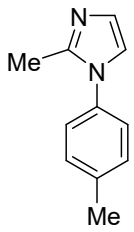

3j

3j: 9.7 mg, 28% yield; ^{1}H-NMR (400 MHz, $CDCl_3$) δ 7.27 (d, *J* = 8.0 Hz, 2H), 7.17 (d, *J* = 8.0 Hz, 2H), 7.01 (d, *J* = 1.2 Hz, 1H), 6.97 (d, *J* = 1.2 Hz, 1H), 2.42 (s, 3H), 2.34 (s, 3H).; ^{13}C-NMR (100 MHz, $CDCl_3$) δ 144.7, 138.1, 135.5, 130.0, 127.4, 125.3, 120.7, 21.0, 13.7

^{1}H and ^{13}C NMR charts were consistent with previously reported data.[4]

Characterization of catalysts

X-ray diffraction (XRD). The X-ray diffraction of the crystal structure was conducted using a Rigaku Miniflex diffractometer. A glass plate was utilized to hold the sample powder, which was then placed within the diffractometer. The X-ray source utilized was Cu Kα, with an acceleration voltage of 40 kV and a current of 15 mA.

X-ray fluorescence (XRF). The determination of Cu loading in the catalyst was carried out via XRF analysis using PANalytical Epsilon 1 instrumentation. Prior to the measurements, the Cu-containing sample was mixed with an internal standard of 99.8% pure NiO (Aldrich). The mixing ratio of the catalyst to NiO was 50wt%. The acquired data was analyzed using the fundamental parameter method, employing Omnian software (PANalytical). Table S1 shows the lists of CuO loadings which were approximately 1 mmol g_{cat}^{-1}.

Table S1 Cu content of the prepared catalysts.

Sample	Cu content [mmol g_{cat}^{-1}]
CuO/TiO_2	1.0
CuO/Al_2O_3	1.2
CuO/*m*-ZrO_2	1.1
CuO/*t*-ZrO_2	1.1

Temperature programmed reduction by H_2 (H_2-TPR). H_2-TPR measurements were conducted by a MicrotracBEL BELCAT-II to evaluate the reducibility of the catalysts. Before the measurement, 40 mg of the sample was heated in an Ar gas flow (Ar) at 300 °C for 1 h. After cooling the sample to room temperature, changing the gas to 5% H_2/Ar, and the signal of TCD became stable, the measurement was started. The heating rate was set to 5 °C min^{-1}.

Scanning transmission electron microscopy (STEM). The particle morphology was investigated by an ultra-high resolution scanning transmission electron microscope (JEOL JEM-ARM200F) equipped with a spherical aberration corrector for a STEM probe. The sample was dispersed in ethanol (Wako, purity > 99.5%) and the suspension was dropped onto a carbon-coated molybdenum grid (Ohken shoji Co., NP-M15) to deposit the particles on the microgrid film of the grid. Elemental maps of Cu and Zr were recorded using an energy dispersive X-ray (EDX) detector.

X-ray absorption spectroscopy (XAS). Using X-ray absorption spectroscopy (XAS) at the BL14B2 beamline at SPring-8, the Cu K-edge XANES (X-ray absorption near edge structure) and EXAFS (extended X-ray absorption fine structure) was measured. XAS data were collected in the quick mode. The Si (3 1 1) monochromator continuously moved from 25.415° to 22.05° over 313 s for the Cu K-edge. Spectra were collected in the transmission mode using ion chambers filled with an Ar/N_2 mixture on pressed pellets of the samples. The samples and BN were mixed using a mortar and pestle and pressed into a thin disk using a 10 mm die set. Spectra were corrected and normalized using Athena and Artemis.[5] The radial structure function (RSF) was obtained by Fourier transformation of the k^3-weighted experimental $\chi(k)$ function (k = 30-110 nm^{-1}) into the R space. Theoretical phase-shift and amplitude functions were calculated with the FEFF6 program.

Table S2 Parameters calculated by fitting the EXAFS signals of CuO and the prepared Cu-based catalysts shown in **Fig. 2** and **S1** †

Sample	Shell	S_0^2	CN	R / Å	σ^2 / Å^2	ΔE_0 / eV	R factor
CuO	Cu-O	0.810±0.112	4 *	1.96±0.01	0.004±0.001	3.48±1.76	0.007
	Cu-O		2 *	2.76±0.08	0.012±0.015		
	Cu-Cu		4 *	2.91±0.02	0.006±0.001		
	Cu-Cu		4 *	3.10±0.01	0.006±0.002		
CuO/Al_2O_3	Cu-O	0.780±0.097	3.9±0.5	1.95±0.01	0.005±0.001	2.40±1.61	0.019
	Cu-O		1.9±0.2	2.89±0.04	0.009±0.005		
CuO/TiO_2	Cu-O	0.812±0.108	4.0±0.5	1.95±0.01	0.004±0.001	3.04±1.80	0.008
	Cu-O		2.0±0.3	2.73±0.11	0.017±0.019		
	Cu-Cu		4.0±0.5	2.90±0.02	0.007±0.002		
	Cu-Cu		4.0±0.5	3.08±0.03	0.008±0.002		
$CuO/m\text{-}ZrO_2$	Cu-O	0.746±0.123	4.0±0.5	1.95±0.01	0.003±0.002	3.23±2.29	0.012
	Cu-O		2.0±0.3	2.71±0.15	0.018±0.024		
	Cu-Cu		4.0±0.5	2.90±0.03	0.007±0.003		
	Cu-Cu		4.0±0.5	3.08±0.03	0.009±0.003		
$CuO/t\text{-}ZrO_2$	Cu-O	0.793±0.084	3.9±0.4	1.95±0.01	0.006±0.001	1.60±1.44	0.019
$CuO/t\text{-}ZrO_2$ After reaction	Cu-O	0.763±0.080	3.8±0.4	1.95±0.01	0.006±0.001	0.66±1.38	0.018

† Notations: S_0^2, intrinsic loss factor; R, distance; CN, coordination number; σ, Debye-Waller factor; ΔE_0, increase in the threshold energy. Confidence intervals = 68%. * Fixed to the values.

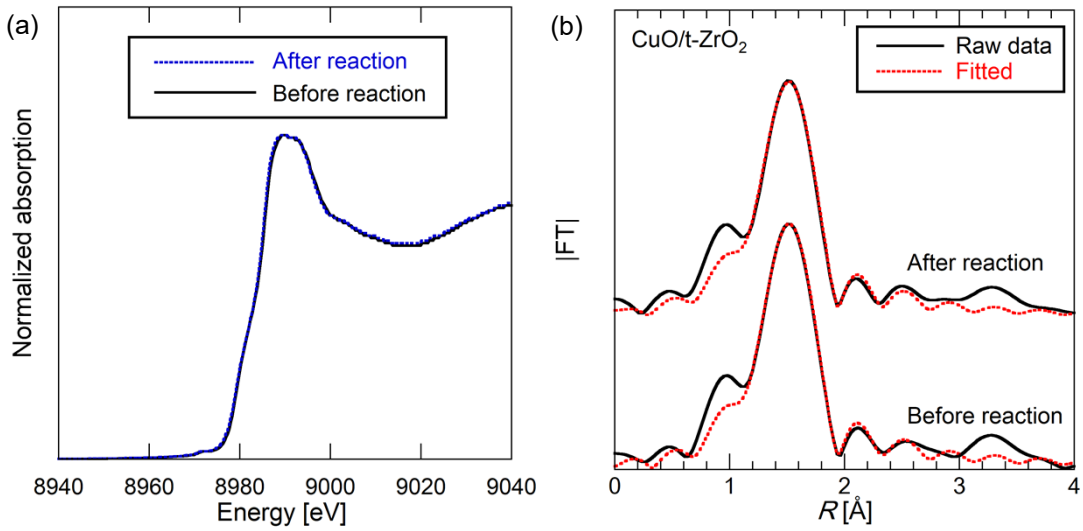

Fig. S1 Cu-K edge XANES spectra for (a) CuO/*t*-ZrO_2 before and after reaction. (b) Fourier transforms of k^3-weighted EXAFS oscillations measured at room temperature near the Cu K-edge of CuO/*t*-ZrO_2 before and after reaction. *k* range: 30-110 nm^{-1}. *R* range: 1.0-3.4 Å.

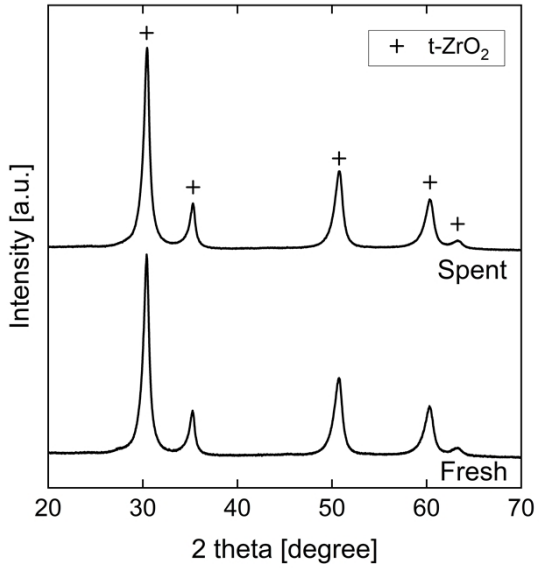

Fig. S2 XRD patterns of fresh and spent CuO/*t*-ZrO_2.

Computational details of DFT calculations

The CuO/*t*-ZrO_2 surface was prepared by starting from the *t*-ZrO_2 surface ($Zr_{96}O_{192}$) shown in **Fig. S3a**. Two Cu atoms were replaced with two surface Zr atoms, resulting in $Zr_{94}Cu_2O_{192}$ (**Fig. S3b**). The two Zr atoms are in the next-nearest neighbor positions with the Cu–Cu distance of 6.19 Å as observed in Fourier transforms of the k^3-weighted EXAFS oscillations in **Fig. 3b**, and are labeled by Zr_S and Zr_W as shown in **Fig. S3b**, because the two species represent the strong and weak Lewis sites, respectively.[6] After geometry optimization of $Zr_{94}Cu_2O_{192}$, Cu_S and Cu_W atoms that were respectively substituted for the Zr_S and Zr_W atoms became 4-fold and 5-fold coordinated. To make an oxygen vacancy at the surface, we removed one O atom among 32 O atoms in the top layer and the geometry was optimized. We performed 32 geometry optimizations and chose the most stable structure with the lowest energy for $Zr_{94}Cu_2O_{191}$ (**Fig. S3c**). Here, the O vacancy was made for the O atom bonded to the Cu atom with 4-fold coordination. The same computations followed and resulted in $Zr_{94}Cu_2O_{190}$ (**Fig. S3d**) and $Zr_{94}Cu_2O_{189}$ (**Fig. S3e**). The surfaces shown in **Figs. S3b, S3c, S3d,** and **S3e** correspond to Cu^{4+}, Cu^{3+}, Cu^{2+}, and Cu^{+}, respectively.[7] In the calculation of adsorption energies, $Zr_{94}Cu_2O_{190}$ (**Fig. S3c**) was employed.

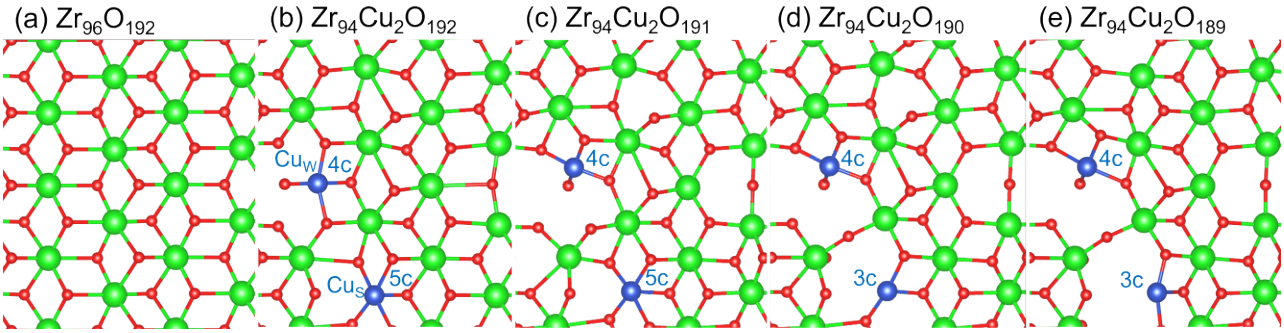

Fig. S3 Top views of (a) *t*-ZrO_2 (101) surface and the Cu-substituted surfaces with (b) zero, (c) one, (d) two, and (e) three oxygen vacancies. The labels of Cu (weak Lewis site, W; strong Lewis site, S) and coordination number (three-fold coordination, 3c; four-fold coordination, 4c; five-fold coordination, 5c) are also shown. Only the top layer is shown for clarity.

Using the calculated energies for the surfaces shown in **Figs. S3b–e**, we estimated the free energy difference of formation from the Cu^{4+} reference state given by previous reports.[7,8]

$$\Delta G = G(Cu^{4-n}) - G(Cu^{4+}) + n\mu_O.$$

Here, $G(Cu^m)$ denotes the free energy for the Cu^m state. The entropic contributions are neglected in this study and approximated by the energies by DFT calculations for the surfaces shown in **Fig. S4**. The chemical potential of oxygen at a given temperature T and pressure p is defined[7,8]

$$\mu_O = \mu_O(T,p^o) + \frac{k_B T}{2}\ln\left(\frac{p}{p^o}\right),$$

where k_B is the Boltzmann constant and p^o is the standard pressure of oxygen ($p^o = 1$ atm). The

energy of oxygen calculated by DFT ($E_{O_2/2}$) was taken as a zero-reference state for μ_O. Since the reaction underwent at 50 ˚C in our experiment, we approximately assumed $\mu_O(T, p^o) = -0.27$ eV (300 K) for the chemical potential of oxygen.[8] **Fig. S4** shows the phase diagram of solid solution by plotting the free energy difference of formation as a function of chemical potential of oxygen. In the O-rich limit (high pressure of oxygen and high μ_O), the energy of Cu^{3+} is lower and the Cu^{3+} state is preferred. On the other hand, the Cu^{2+} state becomes more stable toward the O-poor limit (low μ_O). This indicates that Cu^{2+} and Cu^{3+} species are present at the CuO/*t*-ZrO_2 surface under O-rich conditions, agreeing with the proposed reaction mechanism in **Fig. 10**. Moreover, these results are consistent with the reduced catalytic reactivity observed in the reaction test (**Table 1**). Notably, at the calcination temperature of the catalyst, the formation energies shifted to the left side in **Fig. S4**, with the Cu^{2+} species being the more predominant as observed in the H_2-TPR results. In addition, when Cu^{2+} was oxidized to Cu^{3+}, the atomic charges of the O atoms bonded with Cu atoms decrease from −0.45 to −0.50 on average. The more negatively charged O atoms around the Cu^{2+} cations may be more reducible as measured in the H_2-TPR experiment, and such tendency was also observed for the other Cu-doped oxides.[9]

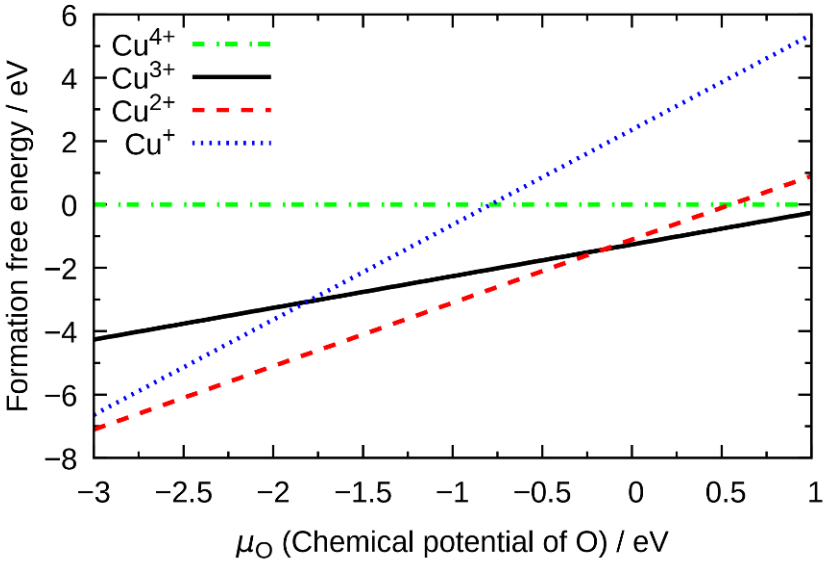

Fig. S4 Formation free energy of the CuO/*t*-ZrO_2 surfaces as a function of the chemical potential of O atom for Cu^{4+}, Cu^{3+}, Cu^{2+}, and Cu^{+} oxidation states at the reaction temperature.

Control experiment

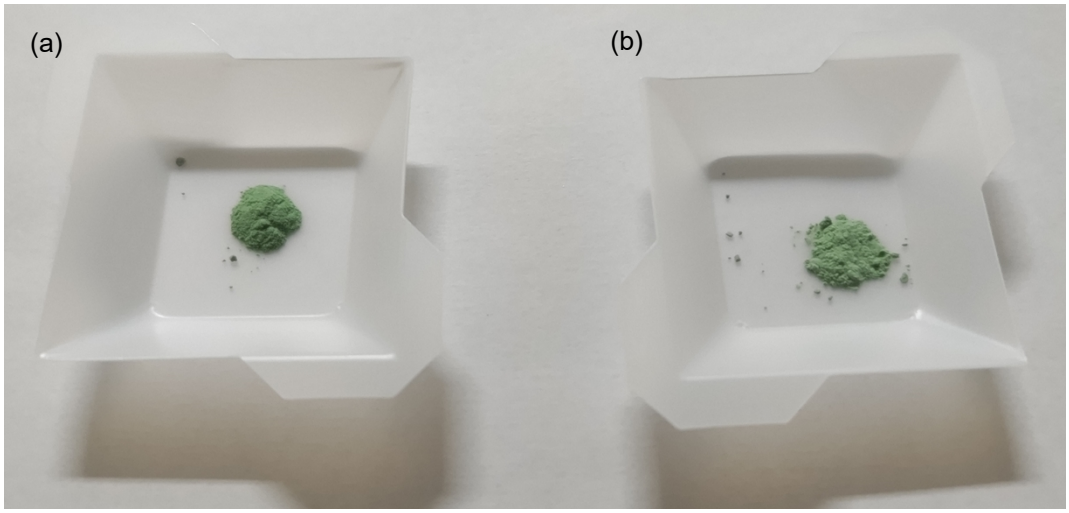

Fig. S5 Colors of CuO/*t*-ZrO_2 (a) before MeOH was added, (b) after stirring in MeOH for 8 h at 50 °C.

References

1. K. Inamoto, K. Nozawa, J. Kadokawa and Y. Kondo, *Tetrahedron* 2012, **68**, 7794.
2. H. X. Li, W. Zhao, H. Y. Li, Z. L. Xu, W. X. Wang and J. P. Lang, *Chem. Commun.,* 2013, **49**, 4259.
3. Y. Wang, Y. Zhang, B. Yang, A. Zhang and Q. Yao, *Org. Biomol. Chem.*, 2015, **13**, 4101
4. B. Ravel and M. Newville, *J. Synchrotron Radiat.,* 2005, **12**, 537.
5. S. Tada, N. Ochiai, H. Kinoshita, M. Yoshida, N. Shimada, T. Joutsuka, M. Nishijima, T. Honma, N. Yamauchi, Y. Kobayashi, et al. *ACS Catalysis,* 2022, **12**, 7748.
6. (a) F. Haase and J. Sauer, *J. Am. Chem. Soc.,* 1998, **120**, 13503; (b) M. Delarmelina, G. Deshmukh, A. Goguet, C. R. A. Catlow and H. Manyar, *J. Phys. Chem. C,* 2021, **125**, 27578.
7. J. S. Elias, N. Artrith, M. Bugnet, L. Giordano, G. A. Botton, A. M. Kolpak and Y. Shao-Horn, *ACS Catal.,* 2016, **6**, 1675.
8. K. Reuter and M. Scheffler, M. *Phys. Rev. B,* 2001, **65**, 035406.
9. T. Joutsuka, R. Hamamura, K. Fujiwara, T. Honma, M. Nishijima and S. Tada, *Int. J. Hydrog. Energy,* 2022, **47**, 21369.

NMR Charts

^{1}H-NMR (400 MHz, $CDCl_3$) chart of **3a**

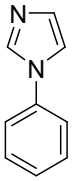

3a

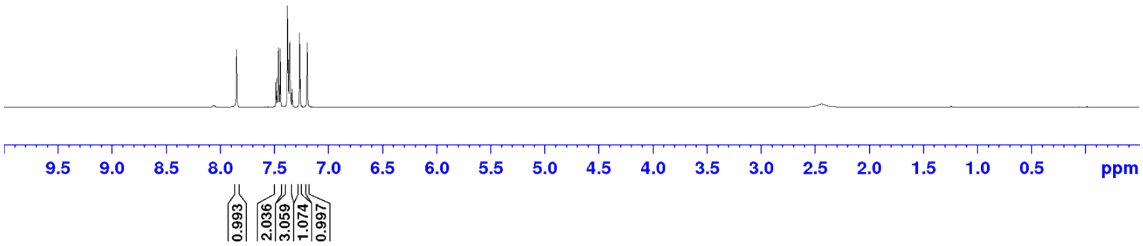

^{13}C-NMR (100 MHz, $CDCl_3$) chart of **3a**

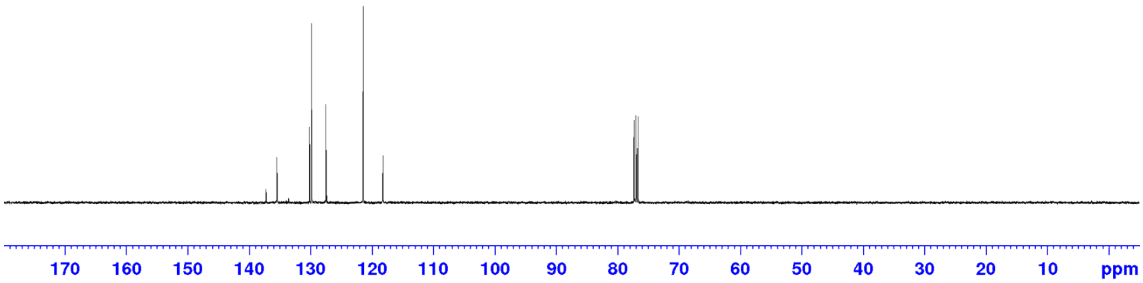

^{1}H-NMR (400 MHz, $CDCl_3$) chart of **3b**

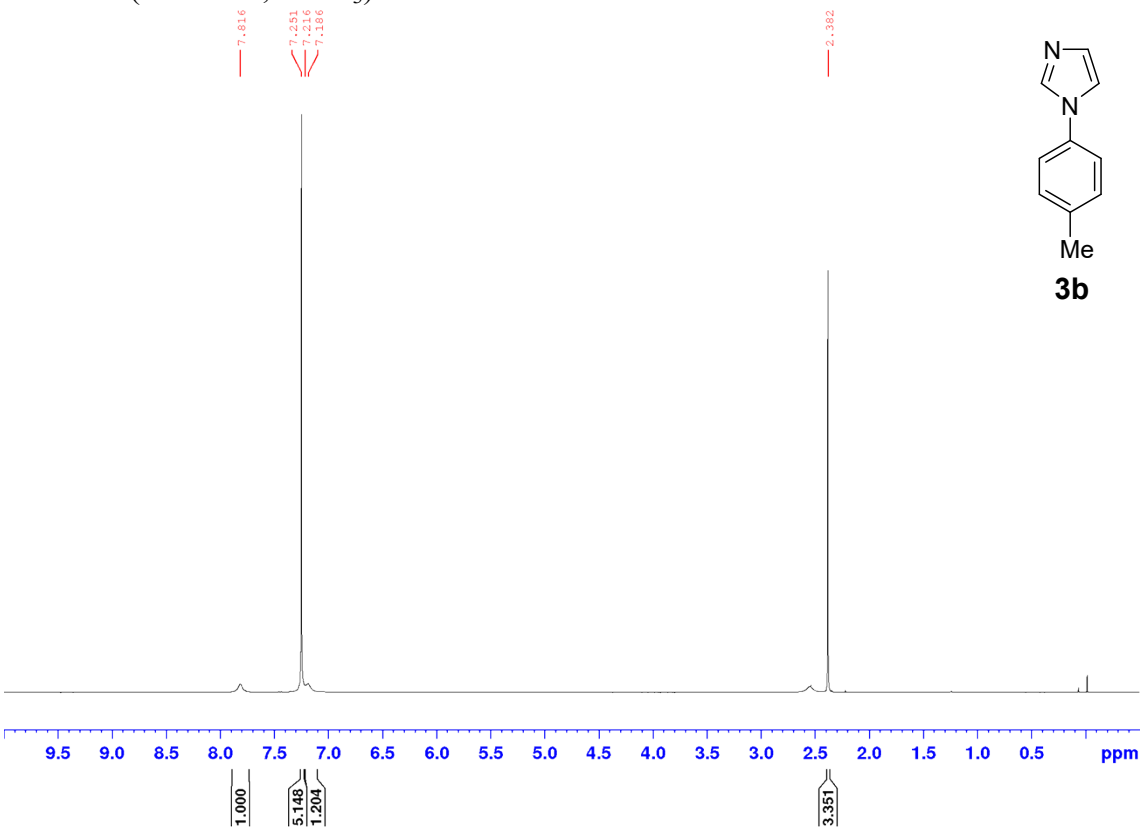

^{13}C-NMR (100 MHz, $CDCl_3$) chart of **3b**

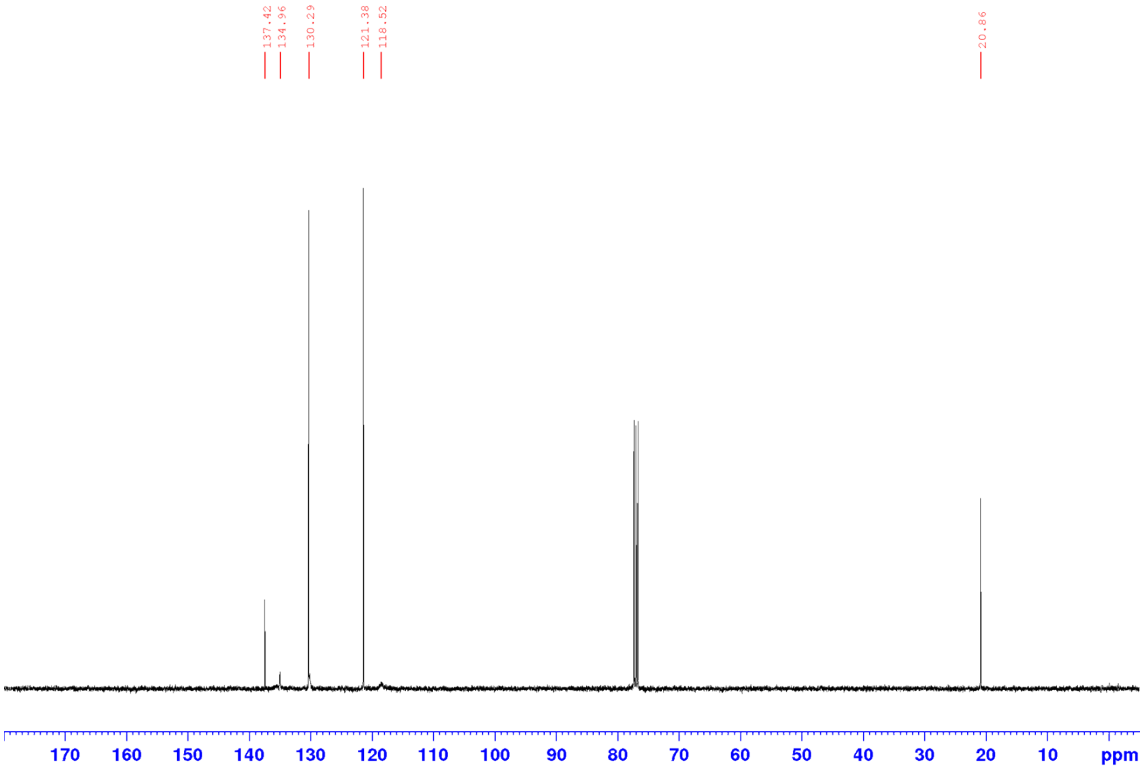

^{1}H-NMR (400 MHz, $CDCl_3$) chart of **3c**

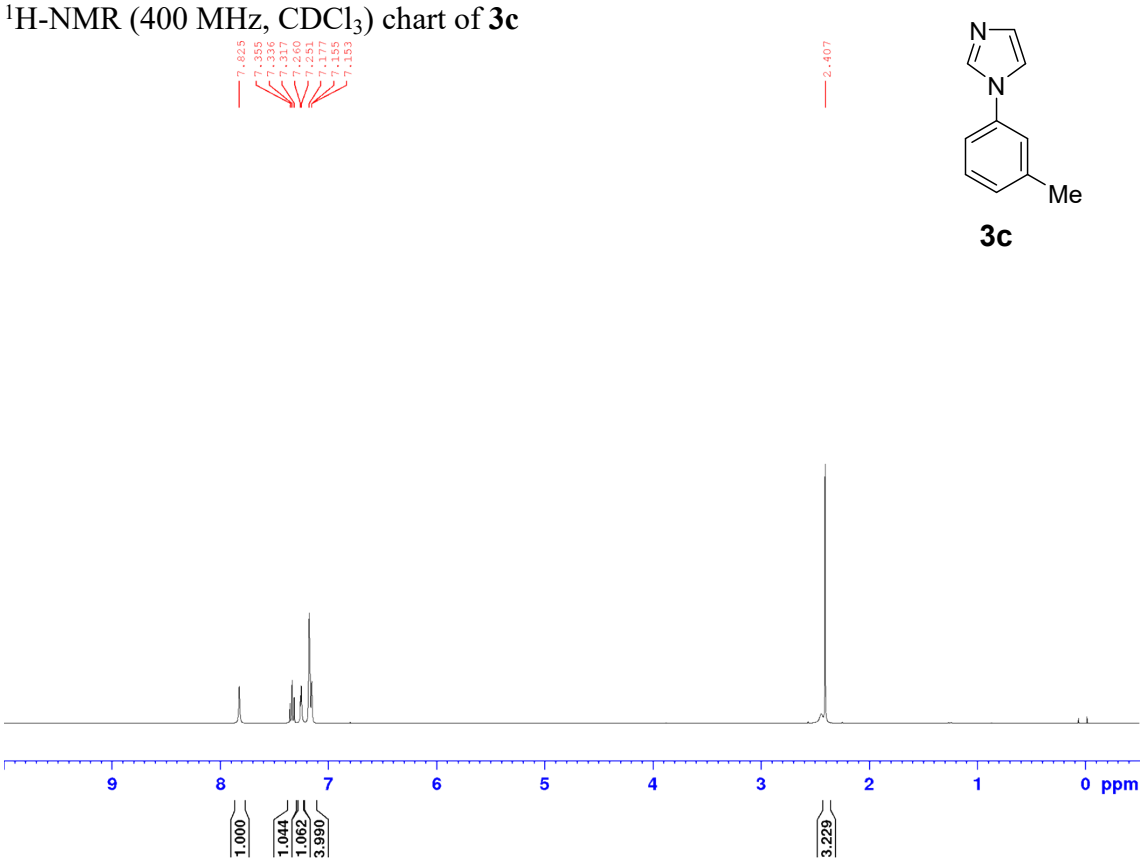

3c

^{13}C-NMR (100 MHz, $CDCl_3$) chart of **3c**

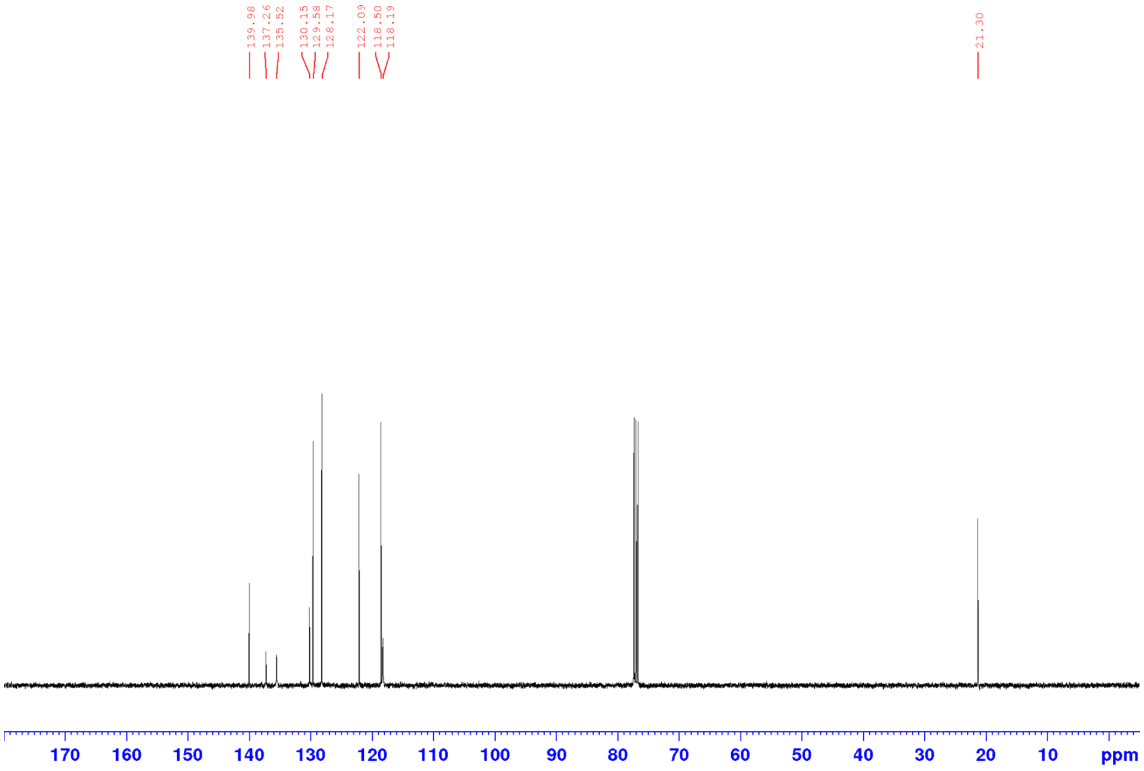

^{1}H-NMR (400 MHz, $CDCl_3$) chart of **3d**

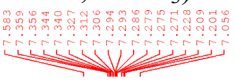

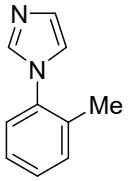

3d

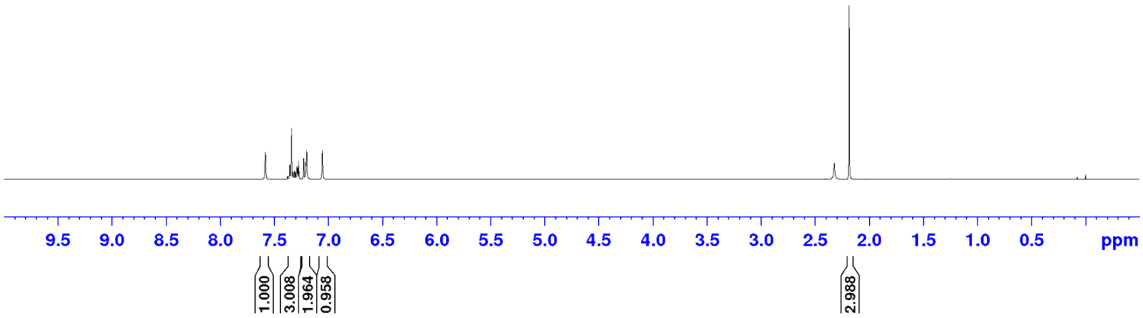

^{13}C-NMR (100 MHz, $CDCl_3$) chart of **3d**

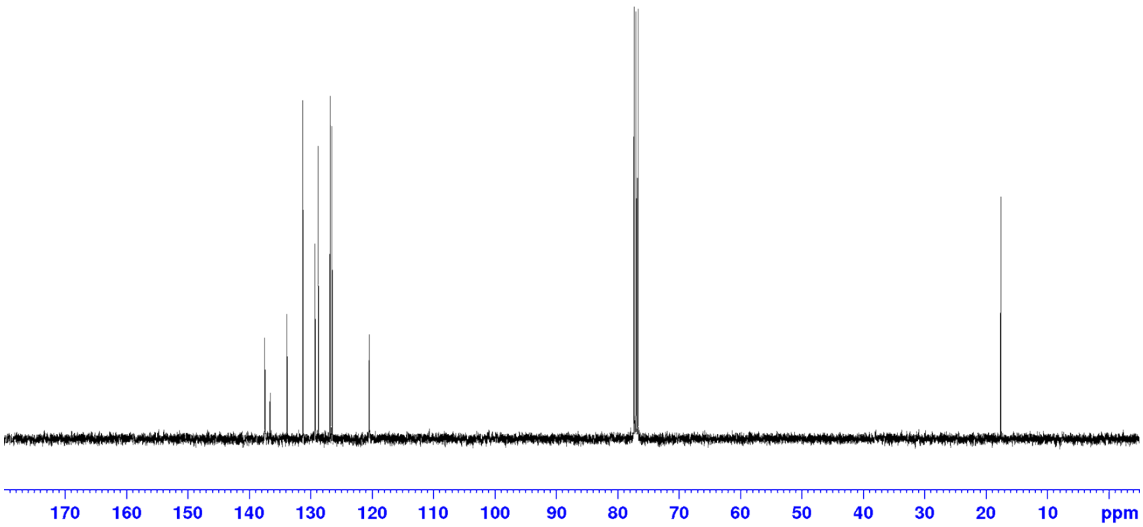

^{1}H-NMR (400 MHz, $CDCl_3$) chart of **3e**

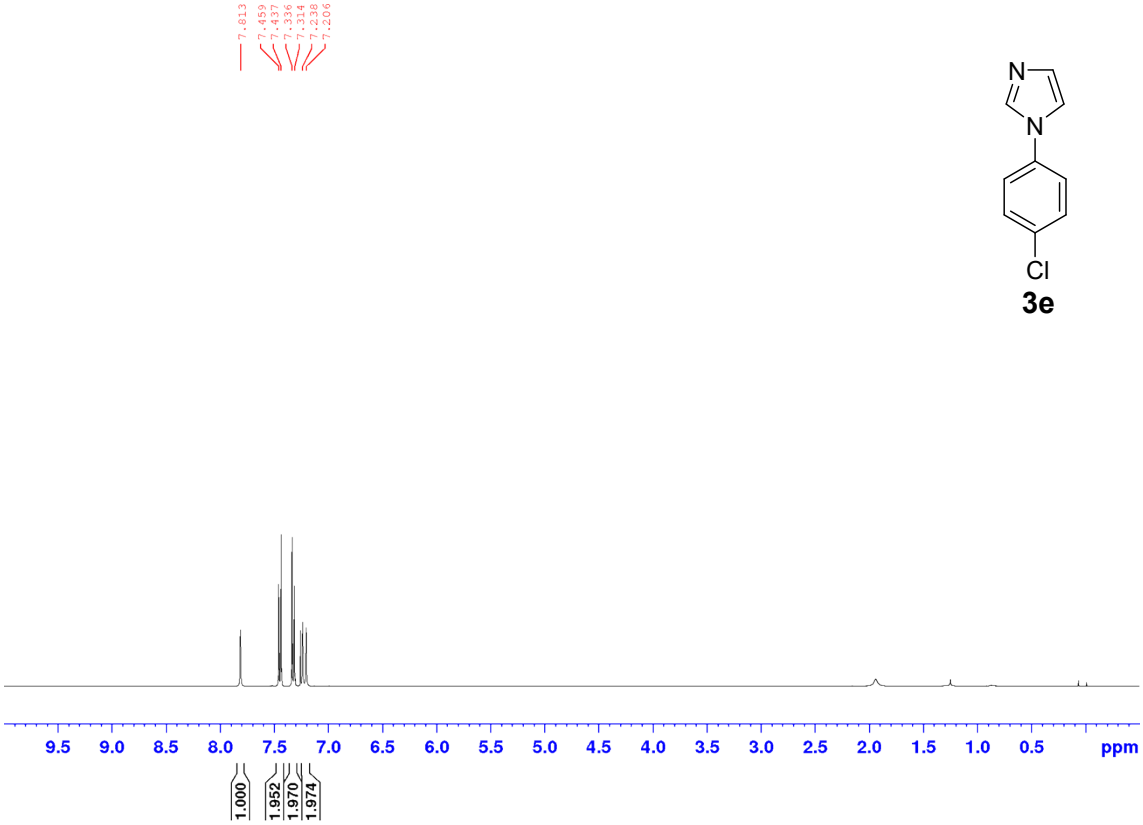

^{13}C-NMR (100 MHz, $CDCl_3$) chart of **3e**

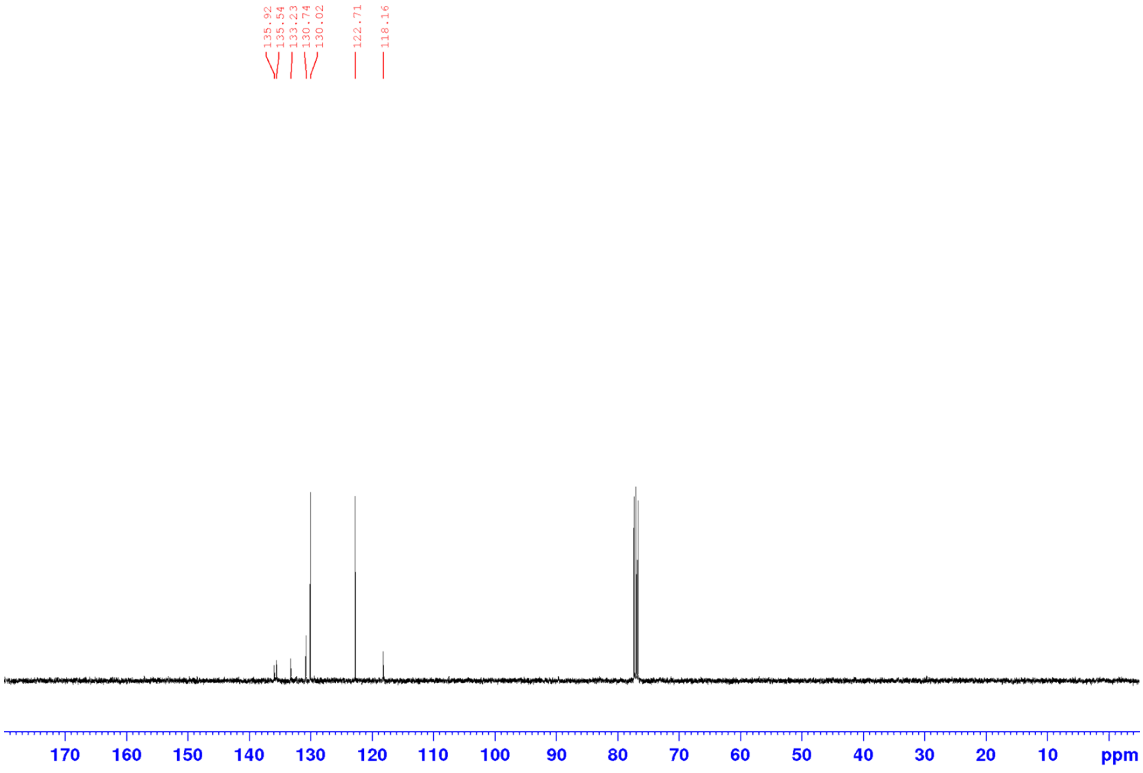

^{1}H-NMR (400 MHz, $CDCl_3$) chart of **3f**

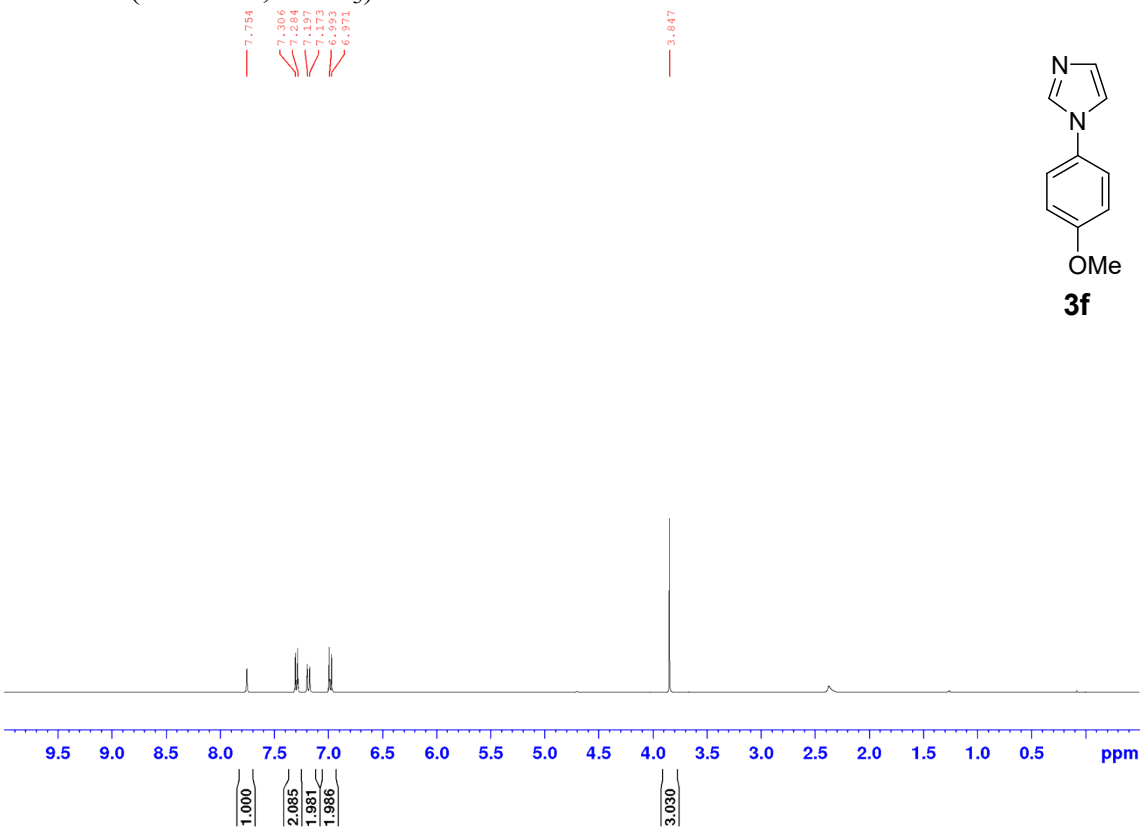

^{13}C-NMR (100 MHz, $CDCl_3$) chart of **3f**

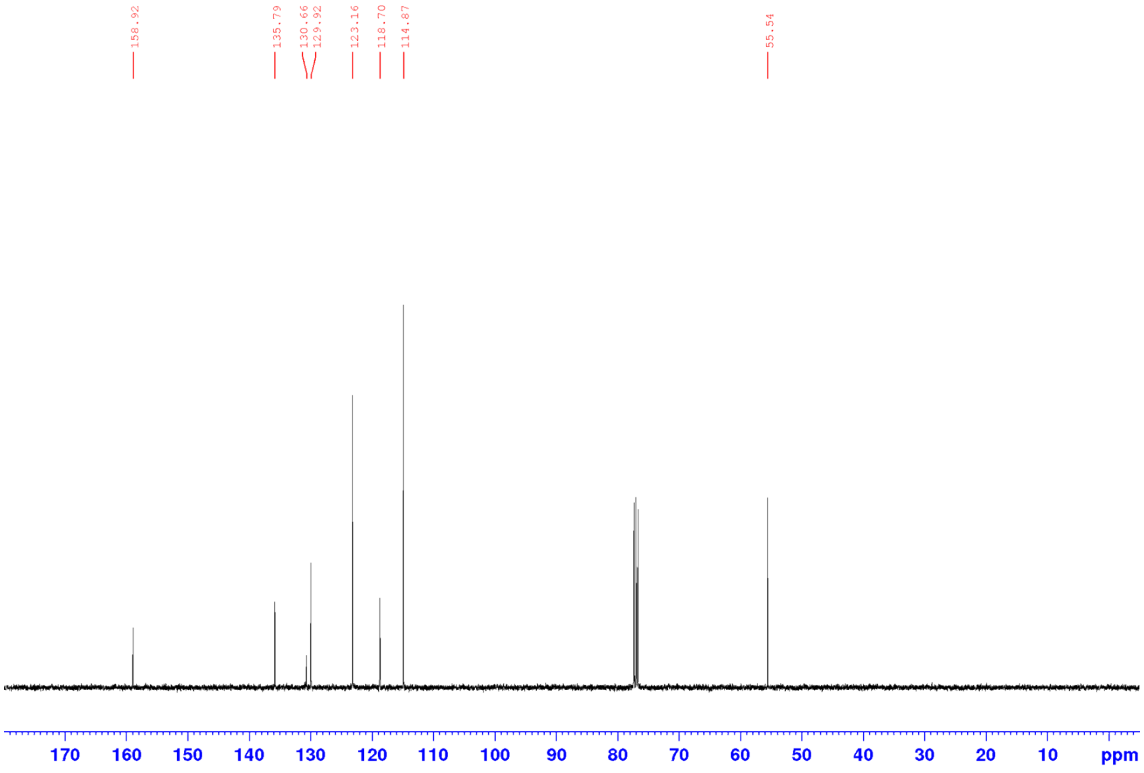

^{1}H-NMR (400 MHz, $CDCl_3$) chart of **3g**

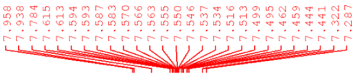

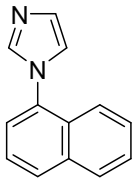

3g

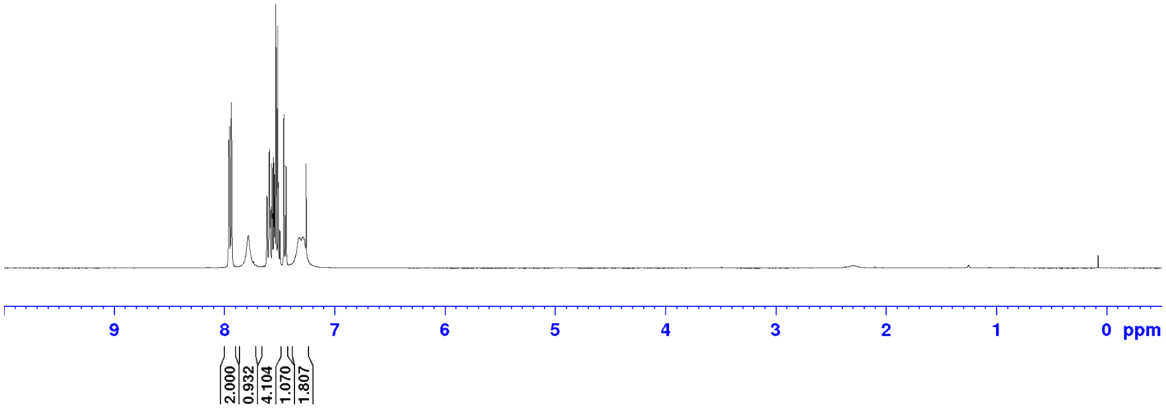

^{13}C-NMR (100 MHz, $CDCl_3$) chart of **3g**

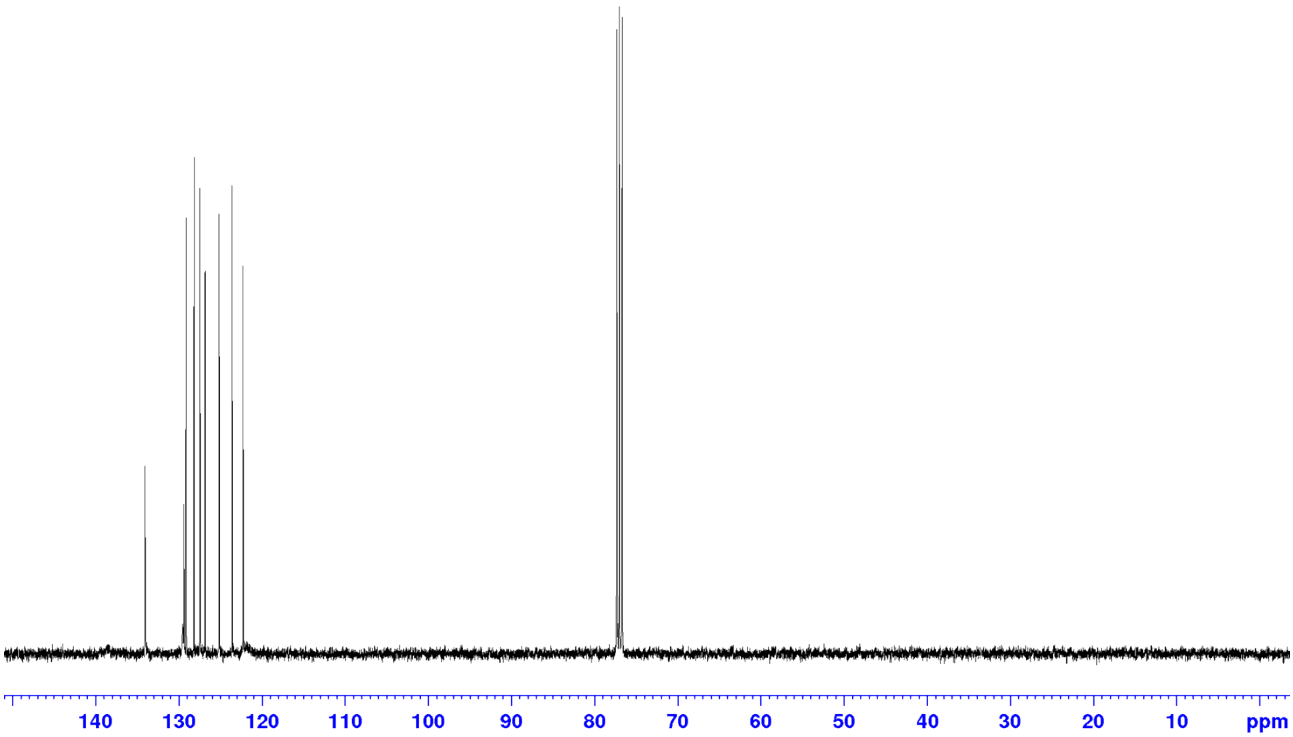

^{1}H-NMR (400 MHz, $CDCl_3$) chart of **3h**

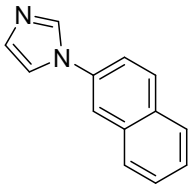

3h

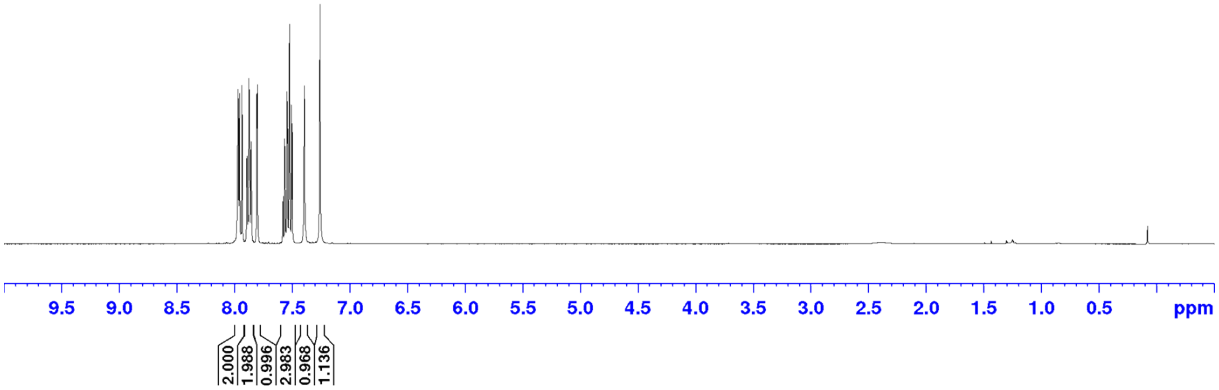

^{13}C-NMR (100 MHz, $CDCl_3$) chart of **3h**

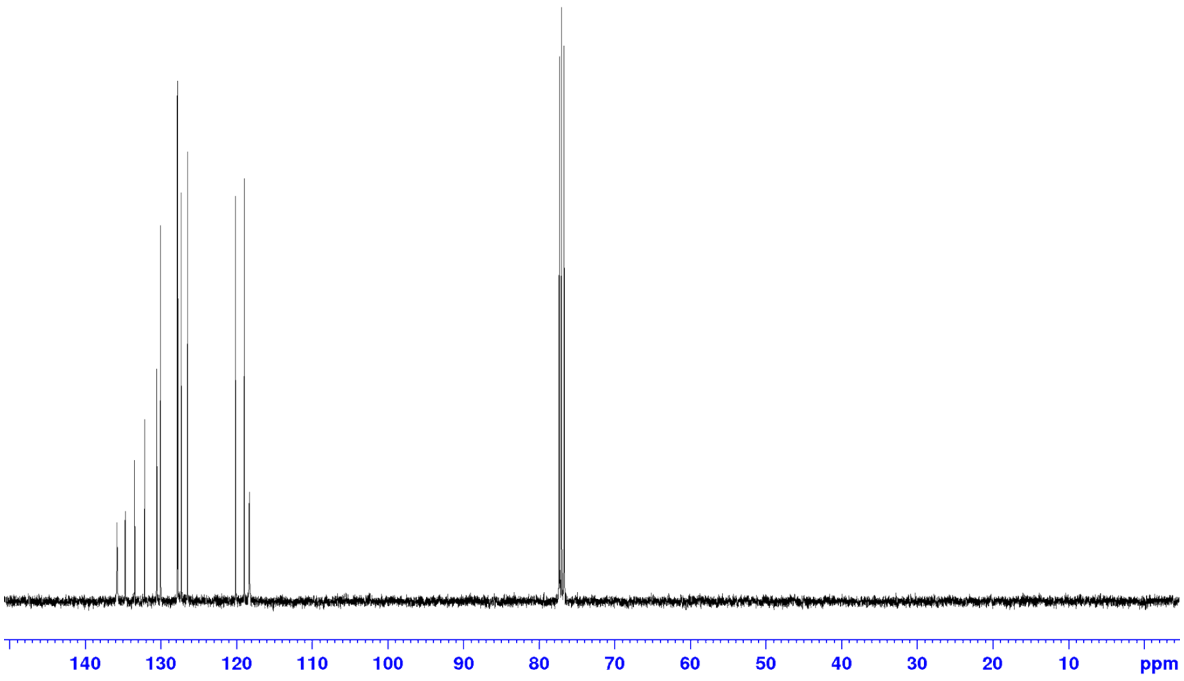

^{1}H-NMR (400 MHz, $CDCl_3$) chart of **3i**

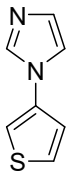

3i

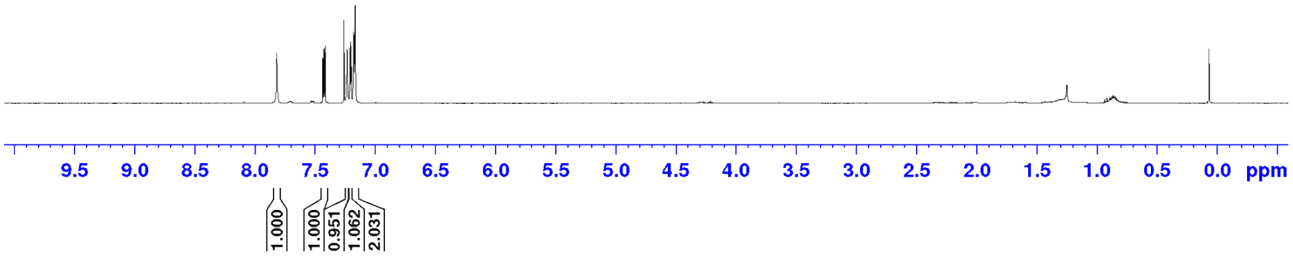

^{13}C-NMR (100 MHz, $CDCl_3$) chart of **3i**

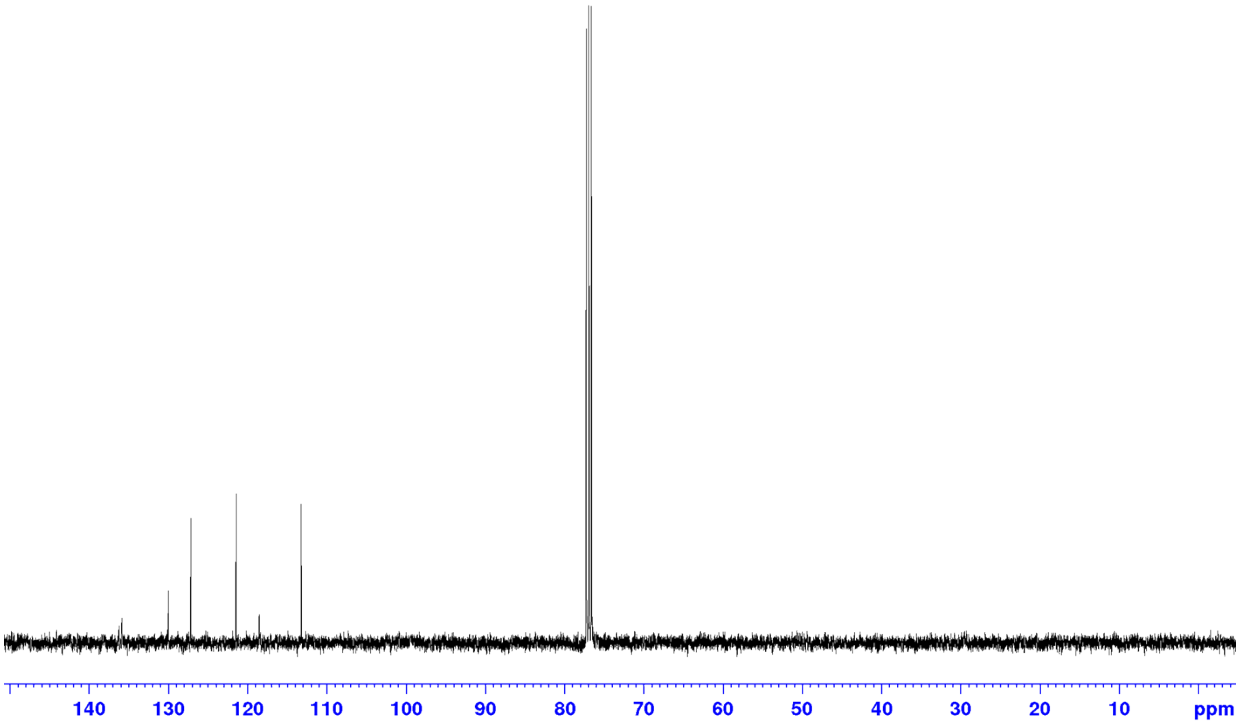

^{1}H-NMR (400 MHz, $CDCl_3$) chart of **3j**

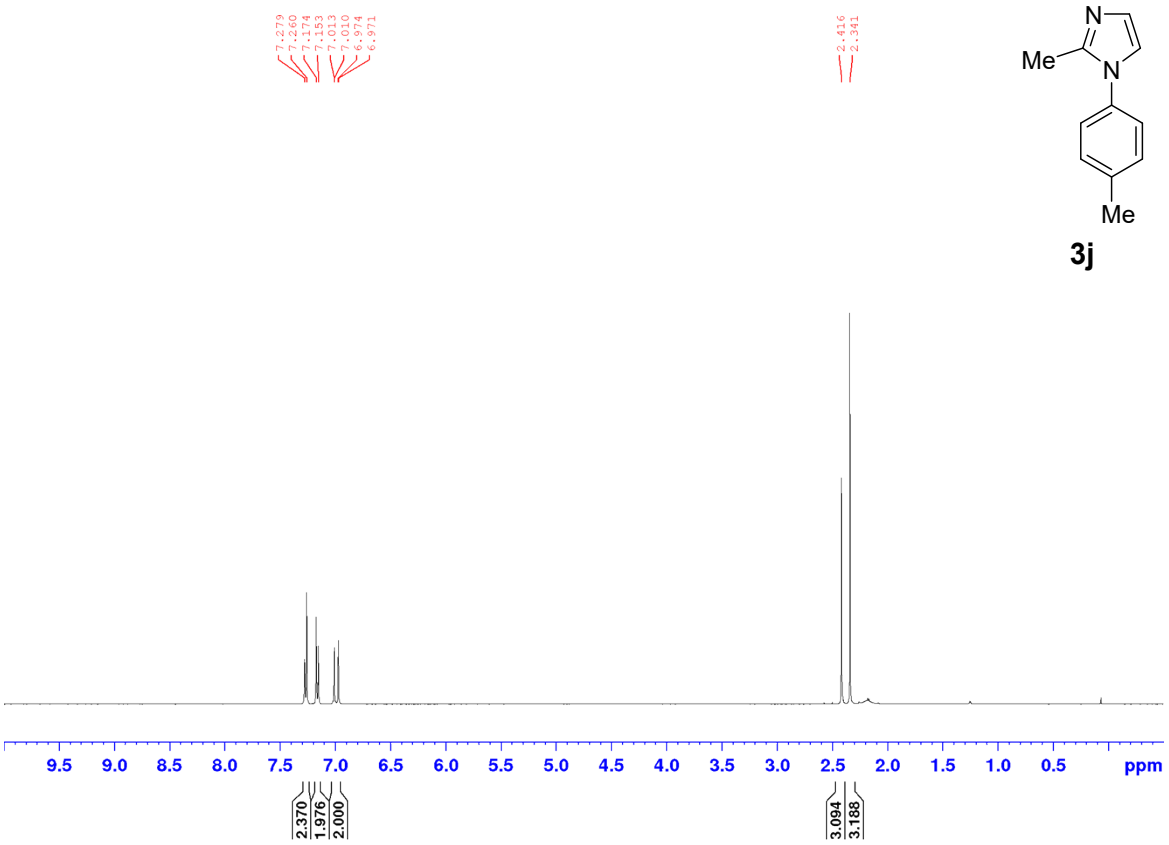
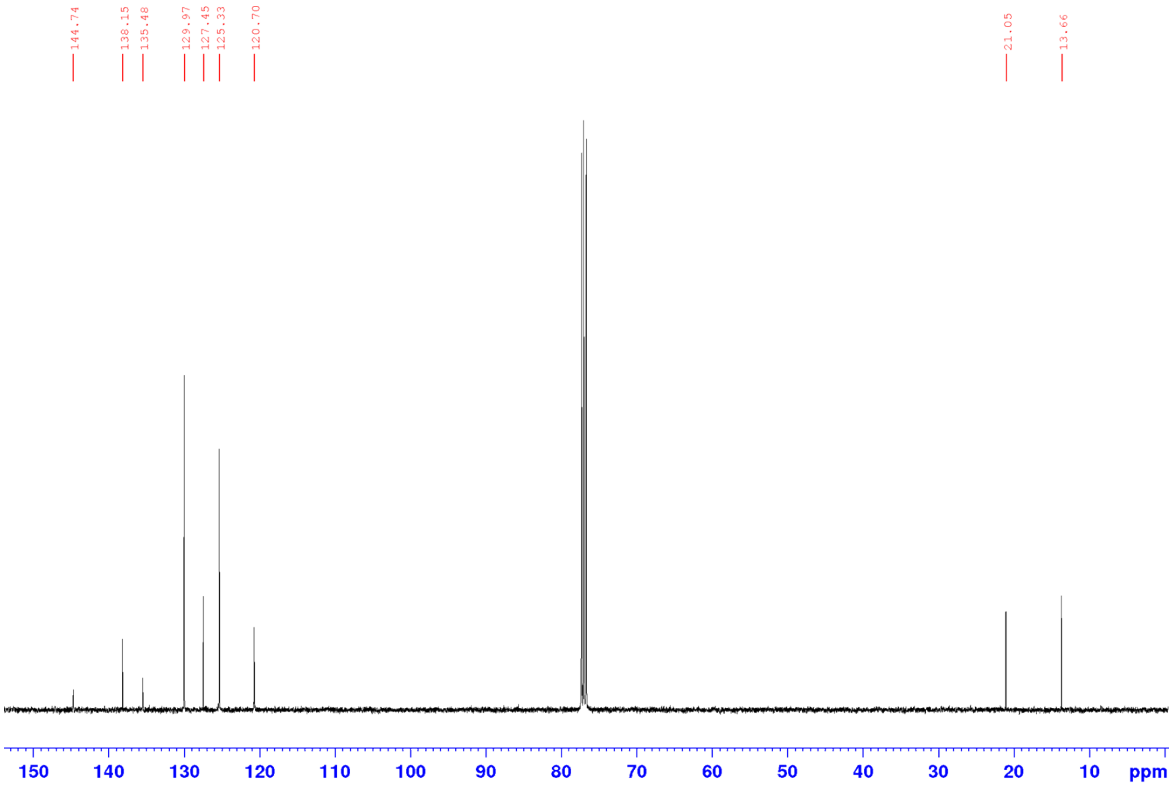
^{13}C-NMR (100 MHz, $CDCl_3$) chart of **3j**